INTERNATIONAL JOURNAL FOR NUMERICAL METHODS IN FLUIDS
Int. J. Numer. Meth. Fluids 2007; **54**:1351–1368
Published online 21 February 2007 in Wiley InterScience (www.interscience.wiley.com). DOI: 10.1002/fld.1431

Explicit formulations for evaluation of velocity gradients using boundary-domain integral equations in 2D and 3D viscous flows

Xiao-Wei Gao*, †

Department of Engineering Mechanics, Southeast University, Nanjing 210096, People's Republic of China

SUMMARY

In this paper, explicit boundary-domain integral equations for evaluating velocity gradients are derived from the basic velocity integral equations. A free term is produced in the new strongly singular integral equation, which is not included in recent formulations using the complex variable differentiation method (CVDM) to compute velocity gradients (*Int. J. Numer. Meth. Fluids* 2004; **45**:463–484; *Int. J. Numer. Meth. Fluids* 2005; **47**:19–43). The strongly singular domain integrals involved in the new integral equations are accurately evaluated using the radial integration method (RIM). Considerable computational time for evaluating integrals of velocity gradients can be saved by using present formulation than using CVDM. The formulation derived in this paper together with those presented in reference (*Int. J. Numer. Meth. Fluids* 2004; **45**:463–484) for 2D and in (*Int. J. Numer. Meth. Fluids* 2005; **47**:19–43) for 3D problems constitutes a complete boundary-domain integral equation system for solving full Navier–Stokes equations using primitive variables. Three numerical examples for steady incompressible viscous flow are given to validate the derived formulations. Copyright © 2007 John Wiley & Sons, Ltd.

Received 5 January 2006; Revised 2 October 2006; Accepted 24 November 2006

KEY WORDS: viscous flow; Navier–Stokes equations; boundary element method (BEM); complex variable differentiation method (CVDM); fundamental solution

1. INTRODUCTION

In the last few decades, significant developments have been made in numerical analysis of viscous fluid flows using the boundary element method (BEM) [1–11]. The distinct advantages of BEM over other numerical methods such as the finite difference method (FDM), finite volume method (FVM) and finite element method (FEM) can be identified as follows: (1) the velocity gradient formulation can be explicitly derived from the velocity integral equation. Therefore, the computational accuracy of the velocity gradient is as high as that of the velocity itself (e.g. [1, 2]). However, in other

*Correspondence to: Xiao-Wei Gao, Department of Engineering Mechanics, Southeast University, Nanjing 210096, People's Republic of China.
†E-mail: xwgao@seu.edu.cn

methods such as the ones mentioned above, the accuracy of the velocity gradient is usually one order lower than that of the velocity itself; (2) the boundary conditions at the infinite distance are automatically satisfied in BEM formulations and, consequently, make BEM inherently suitable for solving aerodynamic problems.

Earlier works using the boundary integral equation approach to solve fluid flow problems may be traced back to the work of Wu [3] by partitioning the mass and momentum conservation equations into kinematic and kinetic parts. Several numerical schemes were developed from the stream function–vorticity formulation of Onishi *et al*. [4], velocity–vorticity formulation of Skerget *et al*. [5] and Ramsak and Skerget [6], penalty formulation of Grigoriev and Fafurin [7].

The work using primitive variables to solve two-dimensional (2D) viscous flow problems was carried out by Florez and Power [8]. Honkala and Banerjee utilized a different type of fundamental solution to solve thermoviscous flow problems [9]. Further developments can be found in the works by Sarler and Kuhn [10], and Power and Mingo [11].

The conventional BEM algorithm results in a fully populated coefficient matrix for the system of equations which is very time consuming to solve. In view of this, some new approaches have been developed, such as the meshless local boundary integral equation method [12, 13] and the mesh-based localized boundary-domain integral equation method [14]. In these methods, special fundamental solutions are constructed, which take effect within a localized region for each collocation point. Since a sparse system of equations can be obtained by using these methods, they are competitive with the FEM in solving the system of algebraic equations.

Recently, Gao developed a general boundary-domain integral equation approach using primitive variables for solving 2D [1] and 3D [2] full Navier–Stokes equations based on a reciprocal theorem for Newtonian flows. This approach results in integral equations expressed in terms of velocity, traction and pressure, and are valid for steady, unsteady, compressible and incompressible flows. In this approach, no velocity gradients appear in the integral equations and, through incorporating the divergence of velocity in the continuity equation, the pressure term can be explicitly eliminated from the final system of equations.

In the former works [1, 2] mentioned, in order to avoid the evaluation of strongly singular domain integrals, the divergence of velocity is computed using the complex variable differentiation method (CVDM) [15], which was introduced in BEM for the first time by Gao *et al*. [16]. Although no strongly singular domain integrals need to be performed in the use of CVDM, much computational time is consumed in the computation of velocity gradients since related weakly singular domain integrals need to be evaluated twice for 2D and thrice for 3D problems. Besides, related variables need to be declared as the complex kind, which doubles the memory storage.

This paper presents an explicit integral equation for computing velocity gradients, which is manipulated in the real number space, and therefore can save considerable computational time compared to the use of CVDM. Since the derived boundary-domain integral equations for the velocity gradient include strongly singular domain integrals, a free term will be produced in the establishment of domain integrals when interpreted in the Cauchy principal value sense. The strongly singular domain integrals will be accurately evaluated through a singularity separation technique, in which the radial integration method (RIM) [17] is used to remove the strong singularity. In Section 2, the basic boundary-domain integral equations for velocity developed in [1, 2] will be reviewed. The correspondence of the related fundamental solutions to those used in elasticity BEM is also discussed in this section. Full formulations for the velocity gradient will be presented in Section 3 and reduced to the pressure computation equation in Section 4. Section 5 will present regularized formulations for evaluating strongly singular domain integrals included in the velocity

DOI: 10.1002/fld

gradient integral equations. A brief description of the numerical implementation of the derived formulations will be given in Section 6 and three numerical examples will be reported in Section 7 to demonstrate the correctness of the derived formulations, following which is a concluding remark.

2. VELOCITY BOUNDARY-DOMAIN INTEGRAL EQUATIONS FOR VISCOUS FLOWS

In viscous fluid mechanics, the governing equations can be written as [18]

Continuity equation:

$$\frac{\partial \rho}{\partial t} + \frac{\partial \rho u_i}{\partial x_i} = 0 \tag{1}$$

Momentum equations:

$$\frac{\partial \rho u_i}{\partial t} + \frac{\partial \rho u_i u_j}{\partial x_j} = \frac{\partial \sigma_{ij}}{\partial x_j} + \rho b_i \tag{2}$$

where t is the time, ρ the fluid density, and u_i the ith velocity component, b_j the body force per unit mass (e.g. the gravity force) and σ_{jk} the stress tensor, and repeated subscripts stand for summation. For Newtonian fluids, the constitutive relationship between the stresses and velocities based on Stokes' hypothesis can be expressed as

$$\sigma_{ij} = -p\delta_{ij} + \mu\left(\frac{\partial u_i}{\partial x_j} + \frac{\partial u_j}{\partial x_i}\right) - \frac{2}{3}\mu\frac{\partial u_k}{\partial x_k}\delta_{ij} \tag{3}$$

where $p = -\sigma_{ii}/3$ is the pressure, δ_{ij} the Kronecker delta function, μ the viscosity (constant here).

On the fluid boundary with outward normal n_i, the relationship between the stress and traction t_i (force per unit area) can be expressed as

$$t_i = \sigma_{ij} n_j \tag{4}$$

From these equations, the reciprocal work theorem for viscous fluid flow can be derived [1] and, based on this theorem, a boundary-domain integral equation for 2D and 3D can be derived as follows [1, 2]:

$$\begin{aligned} u_i(x) = &\int_\Gamma u^*_{ij}(x, y) t_j(y)\, \mathrm{d}\Gamma(y) - \int_\Gamma t^*_{ij}(x, y) u_j(y)\, \mathrm{d}\Gamma(y) \\ &- \int_\Gamma u^*_{ij}(x, y) n_k(y) \rho(y) u_j(y) u_k(y)\, \mathrm{d}\Gamma(y) \\ &+ \int_\Omega u^*_{ij,k}(x, y) \rho(y) u_j(y) u_k(y)\, \mathrm{d}\Omega(y) \\ &+ \int_\Omega u^*_{ij}(x, y) \rho(y) b_j(y)\, \mathrm{d}\Omega(y) - \int_\Omega u^*_{ij}(x, y) \frac{\partial \rho u_j}{\partial t}\, \mathrm{d}\Omega(y) \\ &+ \int_\Omega u^*_{ij,j}(x, y) p(y)\, \mathrm{d}\Omega(y) \end{aligned} \tag{5}$$

DOI: 10.1002/fld

where Γ is the boundary of the problem domain Ω, x denotes the source point and y the field point, $(*)_{,i} = \partial(*)/\partial y_i$. Fundamental solutions appearing in the above equation can be expressed as

$$u^*_{ij}(x, y) = \begin{cases} \dfrac{1}{16\alpha\pi\mu}\left\{7\delta_{ij}\ln\left(\dfrac{1}{r}\right) + r_{,i}\, r_{,j}\right\} & \text{for 2D } (\beta = 2) \\ \dfrac{1}{16\alpha\pi\mu r}\{7\delta_{ij} + r_{,i}\, r_{,j}\} & \text{for 3D } (\beta = 3) \end{cases} \tag{6}$$

$$t^*_{ij}(x, y) = \frac{-1}{8\alpha\pi r^\alpha}\{3(n_i r_{,j} - n_j r_{,i}) + (\beta r_{,i}\, r_{,j} + 3\delta_{ij})n_k r_{,k}\} \tag{7}$$

$$u^*_{ij,k}(x, y) = \frac{-1}{16\alpha\pi\mu r^\alpha}\{7\delta_{ij} r_{,k} - \delta_{ik} r_{,j} - \delta_{jk} r_{,i} + \beta r_{,i}\, r_{,j}\, r_{,k}\} \tag{8}$$

$$u^*_{ij,j} = \frac{-3r_{,i}}{8\alpha\pi\mu r^\alpha} \tag{9}$$

where $\alpha = \beta - 1$ with $\beta = 2$ for 2D and $\beta = 3$ for 3D problems, r is the distance between points x and y, i.e. $r = \|y - x\|$, and

$$r_{,i} = \frac{\partial r}{\partial y_i} = \frac{y_i - x_i}{r} \tag{10}$$

Equation (5) is a general boundary-domain integral equation valid for steady, unsteady, compressible and incompressible flows. Comparing $u^*_{ij}(x, y)$ and $t^*_{ij}(x, y)$ to those used in elasticity BEM [19] shows that the fundamental solutions in the viscous flows correspond to those of elasticity BEM through replacing the shear modulus G and Poisson's ratio v in elasticity BEM using the viscosity μ and -1 in viscous flows, respectively.

It is noted that Equation (5) is only valid for internal source points. For boundary source points, a limiting process needs to be performed and the 'rigid body motion' condition may be applied to determine the strongly singular boundary integrals, as done in the conventional BEM [19, 20].

From Equation (5) it can be seen that except for the traction t_i and velocity u_i, the pressure p appears in the integral equation. To solve these quantities, continuity equation (1) is required to close the equation system and thereby the divergence of velocity $\partial u_i(x)/\partial x_i$ needs to be evaluated. For the general purpose, the velocity gradient expression will be derived in the next section and then the divergence of velocity will be formed by incorporating indices.

3. VELOCITY GRADIENT BOUNDARY-DOMAIN INTEGRAL EQUATIONS FOR VISCOUS FLOWS

Differentiating Equation (5) with respect to the source point x yields

$$\frac{\partial u_i(x)}{\partial x_l} = \int_\Gamma \frac{\partial u^*_{ij}(x, y)}{\partial x_l} t_j(y)\, \mathrm{d}\Gamma(y) - \int_\Gamma \frac{\partial t^*_{ij}(x, y)}{\partial x_l} u_j(y)\, \mathrm{d}\Gamma(y) - \int_\Gamma \frac{\partial u^*_{ij}(x, y)}{\partial x_l} n_k(y)\rho(y) u_j(y) u_k(y)\, \mathrm{d}\Gamma(y)$$

DOI: 10.1002/fld

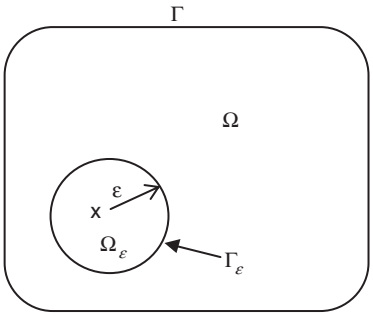

Figure 1. A small domain Ω_ε cut out from Ω.

$$+\int_\Omega \frac{\partial u^*_{ij}(x,y)}{\partial x_l}\,\rho(y)b_j(y)\,\mathrm{d}\Omega(y)-\int_\Omega \frac{\partial u^*_{ij}(x,y)}{\partial x_l}\,\frac{\partial \rho u_j}{\partial t}\,\mathrm{d}\Omega(y)$$
$$+\int_\Omega \frac{\partial u^*_{ij,j}(x,y)}{\partial x_l}\,p(y)\,\mathrm{d}\Omega(y)+\int_\Omega \frac{\partial u^*_{ij,k}(x,y)}{\partial x_l}\,\rho(y)u_j(y)u_k(y)\,\mathrm{d}\Omega(y) \qquad (11)$$

All domain integrals included in the above equation are interpreted in the Cauchy principal value sense except for the last two terms, which result in strongly singular kernels after differentiation and for which special treatments need to be carried out. To do this, let us cut out a small spherical domain Ω_ε from domain Ω with radius ε centred at point x (Figure 1).

Noticing that $\partial(\,)/\partial x_i = -\partial(\,)/\partial y_i = -(\,)_{,i}$, the last integral of Equation (11) can be written as

$$\begin{aligned}\int_\Omega \frac{\partial u^*_{ij,k}(x,y)}{\partial x_l}\,\rho(y)u_j(y)u_k(y)\,\mathrm{d}\Omega(y) &= -\lim_{\varepsilon\to 0}\int_{\Omega-\Omega_\varepsilon} u^*_{ij,kl}(x,y)\rho(y)u_j(y)u_k(y)\,\mathrm{d}\Omega(y)\\ &\quad -\rho(x)u_j(x)u_k(x)\lim_{\varepsilon\to 0}\int_{\Omega_\varepsilon}\frac{\partial u^*_{ij,k}(x,y)}{\partial x_l}\,\mathrm{d}\Omega(y)\\ &= -\int_\Omega u^*_{ij,kl}(x,y)\rho(y)u_j(y)u_k(y)\,\mathrm{d}\Omega(y)\\ &\quad -\rho(x)u_j(x)u_k(x)\lim_{\varepsilon\to 0}\int_{\Gamma_\varepsilon} u^*_{ij,k}(x,y)n_l\,\mathrm{d}\Gamma(y) \qquad (12)\end{aligned}$$

where Γ_ε is the spherical surface of the domain Ω_ε.

Now the domain integral on the right-hand side of Equation (12) is interpreted in the Cauchy principal value sense and the last surface integral in Equation (12) can be easily integrated using Equation (8) as

$$\int_{\Gamma_\varepsilon} u^*_{ij,k}(x,y)n_l\,\mathrm{d}\Gamma(y)=\frac{1}{8\beta\gamma\mu}\{-(\beta+7\gamma)\delta_{ij}\delta_{kl}+2(\delta_{ik}\delta_{jl}+\delta_{jk}\delta_{il})\} \qquad (13)$$

where $\gamma=\beta+2$. Equation (13) gives the coefficient of the free term for the domain integral shown in Equation (12). In a similar manner, the domain integral including pressure p in Equation (11)

DOI: 10.1002/fld

can be derived as

$$\int_\Omega \frac{\partial u^*_{ij,j}(x,y)}{\partial x_l}\, p(y)\,\mathrm{d}\Omega(y) = -\int_\Omega u^*_{ij,jl}(x,y)p(y)\,\mathrm{d}\Omega(y) + \frac{3}{4\beta\mu}\,\delta_{il}p(x) \tag{14}$$

Substituting Equations (12)–(14) into Equation (11), one can obtain the velocity gradient boundary-domain integral equation as

$$\begin{aligned}\frac{\partial u_i(x)}{\partial x_l} = &-\int_\Gamma u^*_{ij,l}(x,y)t_j(y)\,\mathrm{d}\Gamma(y) + \int_\Gamma t^*_{ij,l}(x,y)u_j(y)\,\mathrm{d}\Gamma(y)\\ &+\int_\Gamma u^*_{ij,l}(x,y)n_k(y)\rho(y)u_j(y)u_k(y)\,\mathrm{d}\Gamma(y)\\ &-\int_\Omega u^*_{ij,l}(x,y)\rho(y)b_j(y)\,\mathrm{d}\Omega(y) + \int_\Omega u^*_{ij,l}(x,y)\frac{\partial \rho u_j}{\partial t}\,\mathrm{d}\Omega(y)\\ &-\int_\Omega u^*_{ij,kl}(x,y)\rho(y)u_j(y)u_k(y)\,\mathrm{d}\Omega(y) - \int_\Omega u^*_{ij,jl}(x,y)p(y)\,\mathrm{d}\Omega(y)\\ &+\frac{1}{8\beta\gamma\mu}\{(\beta+7\gamma)\delta_{ij}\delta_{kl}-2(\delta_{ik}\delta_{jl}+\delta_{jk}\delta_{il})\}\rho(x)u_j(x)u_k(x)+\frac{3}{4\beta\mu}\,\delta_{il}p(x)\end{aligned} \tag{15}$$

in which the used fundamental solutions are

$$\begin{aligned}t^*_{ij,l} = \frac{-1}{8\pi\alpha r^\beta}\{&3(n_i\delta_{jl}+n_l\delta_{ij}-n_j\delta_{il}) + \beta[3\,(n_j r_{,i} - n_i r_{,j})r_{,l} + n_l r_{,i}\, r_{,j}]\\ &+\beta r_{,m}\, n_m[\delta_{il}r_{,j}+\delta_{jl}r_{,i}-3\delta_{ij}r_{,l}-\gamma r_{,i}\, r_{,j}\, r_{,l}]\}\end{aligned} \tag{16}$$

$$\begin{aligned}u^*_{ij,kl}(x,y) = \frac{1}{16\alpha\pi\mu r^\beta}\{&\delta_{il}\delta_{jk}+\delta_{ik}\delta_{jl}-7\delta_{ij}\delta_{kl}-\beta(\delta_{ik}r_{,j}\, r_{,l}+\delta_{jk}r_{,i}\, r_{,l}-7\delta_{ij}r_{,k}\, r_{,l}\\ &+\delta_{jl}r_{,i}\, r_{,k}+\delta_{kl}r_{,i}\, r_{,j}+\delta_{il}r_{,j}\, r_{,k}) + \beta\gamma r_{,i}\, r_{,j}\, r_{,k}\, r_{,l}\}\end{aligned} \tag{17}$$

$$u^*_{ij,jl} = \frac{-3}{8\alpha\pi\mu r^\beta}\{\delta_{il} - \beta r_{,i}\, r_{,l}\} \tag{18}$$

All integrals included in Equation (15) are interpreted in the Cauchy principal value sense. The last two terms in Equation (15) are the free terms of the velocity gradient integral equation since they are only dependent on the source point coordinates. It is noted that, in this study, Equation (15) is only used for internal source points. For boundary points, since the kernel $t^*_{ij,l}$ is hyper-singular when the source point x approaches the field point y, directly evaluating its boundary integral may give rise to the numerical overflow problem. Therefore, for boundary points, the velocity gradients are computed using the traction–recovery technique as done in References [1, 2, 20]. On the other hand, even for internal points, the domain integrals with kernels $u^*_{ij,kl}$ and $u^*_{ij,jl}$ are strongly singular. Therefore, special treatments are needed. This will be described later in detail.

The velocity gradients play a very important role in the evaluation of the dissipation function involved in the energy equation and will be described in another paper. Besides, the velocity

DOI: 10.1002/fld

gradient equation (15) is also utilized to compute the divergence of velocity, which is used in the continuity equation to produce the pressure integral equation. This will be described in the next section.

4. PRESSURE EQUATIONS BASED ON CONTINUITY EQUATION

The continuity equation (1) can be written as

$$\frac{\partial \rho}{\partial t} + u_i \frac{\partial \rho}{\partial x_i} + \rho \frac{\partial u_i}{\partial x_i} = 0 \tag{19}$$

In order to use this equation, the divergence of velocity, $\partial u_i / \partial x_i$, needs to be determined. From Equation (15) and noticing that $u^*_{ij,ji} = 0$, it follows that

$$\begin{aligned}\frac{\partial u_i}{\partial x_i} = &- \int_\Gamma u^*_{ij,i}(x, y) t_j(y)\, \mathrm{d}\Gamma(y) + \int_\Gamma t^*_{ij,i}(x, y) u_j(y)\, \mathrm{d}\Gamma(y) \\ &+ \int_\Gamma u^*_{ij,i}(x, y) n_k(y) \rho(y) u_j(y) u_k(y)\, \mathrm{d}\Gamma(y) - \int_\Omega u^*_{ij,ki}(x, y) \rho(y) u_j(y) u_k(y)\, \mathrm{d}\Omega(y) \\ &- \int_\Omega u^*_{ij,i}(x, y) \rho(y) b_j(y)\, \mathrm{d}\Omega(y) + \int_\Omega u^*_{ij,i}(x, y) \frac{\partial \rho u_j}{\partial t}\, \mathrm{d}\Omega(y) \\ &+ \frac{3}{4\beta\mu} \rho(x) u_i(x) u_i(x) + \frac{3}{4\mu} p(x)\end{aligned} \tag{20}$$

where

$$t^*_{ij,i} = \frac{-3}{4\alpha\pi r^\beta} \{\delta_{jl} - \beta r_{,j}\, r_{,l}\} n_l \tag{21}$$

$$u^*_{ij,ki} = u^*_{ji,ik} = \frac{-3}{8\alpha\pi\mu r^\beta} \{\delta_{jk} - \beta r_{,j}\, r_{,k}\} \tag{22}$$

From Equation (20) it can be seen that apart from the free term of p (the last term), no pressure is included in the integrals of Equation (20). Therefore, on substituting Equation (20) into the continuity equation (19), one can obtain the integral equation to compute the pressure p.

It is noted that due to the hyper-singular boundary integral problem, Equation (20) can only be applied to internal points. For boundary points, the traction–recovery method is used and the related formulations have been presented in [2].

5. ACCURATE EVALUATION OF STRONGLY SINGULAR DOMAIN INTEGRALS

The domain integrals included in Equation (15) with kernels $u^*_{ij,kl}$ and $u^*_{ij,jl}$, and in Equation (20) with kernel $u^*_{ij,ki}$ are strongly singular when the source point x tends to the field point y. The singularity separation technique [20] is applied to evaluate these integrals. The essence of the technique is the isolation of the singularity and its transformation into a (local) boundary integral.

DOI: 10.1002/fld

Here, only the domain integral with kernel $u^*_{ij,kl}$ is described. Other domain integrals can be done in a straightforward manner.

The domain integrals included in Equation (15) with kernels $u^*_{ij,kl}$ can be isolated by re-writing the integral in the form

$$\int_\Omega u^*_{ij,kl}(x, y)\rho(y)u_j(y)u_k(y)\,\mathrm{d}\Omega(y) = \int_\Omega u^*_{ij,kl}(x, y)\{\rho(y)u_j(y)u_k(y)-\rho(x)u_j(x)u_k(x)\}\,\mathrm{d}\Omega(y) + \rho(x)u_j(x)u_k(x)\int_\Omega u^*_{ij,kl}(x, y)\,\mathrm{d}\Omega(y) \tag{23}$$

Now, the first integral on the right-hand side is weakly singular and can be integrated numerically through the cell-subdivision technique [20]. The strong singularity has been transferred to the last integral, which can be dealt with using the RIM [17]. Since the kernel $u^*_{ij,kl}$ (see Equation (17)) satisfies the integration condition presented in [17], the last domain integral of Equation (23) can be easily transformed into a boundary integral by RIM as follows:

$$\int_\Omega u^*_{ij,kl}(x, y)\,\mathrm{d}\Omega(y) = \int_\Gamma u^*_{ij,kl}(x, y)r\log(r)\frac{\partial r}{\partial n}\,\mathrm{d}\Gamma(y) \tag{24}$$

Now, because the integration is performed through the boundary of the problem, no singularities occur since the source point is located at an internal point. Since Equation (24) is valid for any closed boundary surrounding the source point x, in a numerical implementation, the integral boundary is usually taken as the outer surfaces of the cells surrounding the source point x as done in [20]. This can save considerable computational time.

6. NUMERICAL IMPLEMENTATION FORMULATIONS FOR STEADY INCOMPRESSIBLE FLOWS

Equations (5), (15) and (20) are general integral equations for viscous flows. The numerical implementation of these equations is exactly the same as in the use of CVDM. For further details, one can refer [1, 2]. It should be pointed out that the pressures appearing in the discretized algebraic equations from Equation (5) can be eliminated by using Equations (19) and (20), such that the final system of equations for incompressible flows only contains the velocities and/or tractions as unknowns. Another feature of the present approach is that the velocities explicitly appear in the system of equations with the maximum order of velocity being quadratic. Therefore, the first and second derivatives of the system of equations with respect to velocities can be easily derived and therefore advanced non-linear equation solvers can be directly used to solve the system of equations. The program HYBRJ [21] using the *modified Powell hybrid algorithm* is adopted in this study, which is able to achieve a very fast convergence in the iteration computation [1, 2].

7. NUMERICAL EXAMPLES

To validate the formulations derived in this paper, three numerical examples for steady incompressible flows are presented in this section. The first two examples are from References [1] for

DOI: 10.1002/fld

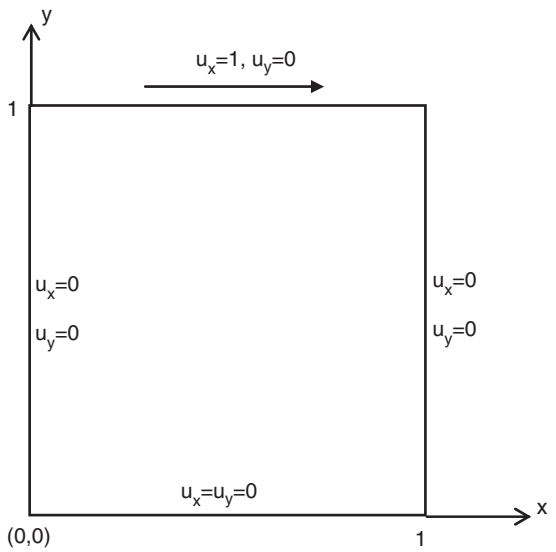

Figure 2. Geometry and boundary conditions for driven cavity flow.

2D and [2] for 3D problems, respectively, with comparisons to the CVDM results, and the third one is a new example with the comparison with ANSYS CFD results.

7.1. Driven flow in an unitary square cavity

The first numerical example concerned is a unitary square cavity (Figure 2). The top side moves with a uniform velocity of 1 unit in the horizontal direction, while the left, right and bottom sides are fixed, including the two corners of the top side. Ghia *et al*. [22] provided a benchmark solution that is used in this example for comparison. Each side of the cavity is discretized into 40 equally spaced linear boundary elements with a total of 160 elements and 160 boundary nodes. The domain of the cavity is approximated with 1600 linear quadrilateral cells with 1521 internal nodes.

The Reynolds number is defined as $Re = \rho U H/\mu$, where U is the characteristic velocity and H the characteristic length. In this example, the parameters are set as $\rho = 100$, $U = 1$, $H = 1$, and $\mu = 1$. This implies that $Re = 100$. Figure 3 shows the computed horizontal velocities on the vertical centreline of the cavity and Figure 4 depicts the vertical velocity profile on the horizontal centre line. Figure 5 gives the velocity vector plot. The computed vortex centre is (0.6112, 0.7351), which is close to the result (0.6172, 0.7344) by Ghia *et al*. [22].

Comparison of the current results with those of CVDM [1] and benchmark solutions [22] (see Figures 3 and 4) shows that the formulations derived in this paper are correct. The current results are so close to those of CVDM that it is very difficult to identify their discrepancy visually.

7.2. Curved pipe flow

The second example deals with the fluid flowing through a 3D curved circular pipe with radius $r = 1$ (Figure 6). The curvature of the pipe is determined by a radius of $R = 9$. The fluid with the property of $\mu = 1$ and $\rho = 1$ is subjected to a vertical body force of $b_z = -10$ and a pressure

DOI: 10.1002/fld

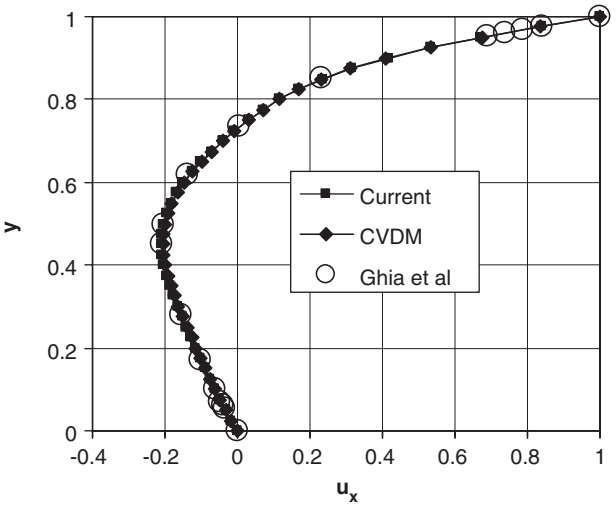

Figure 3. Horizontal velocity profile on vertical centreline.

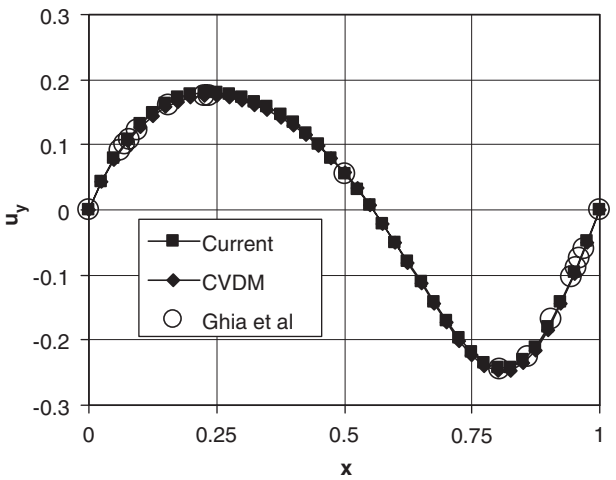

Figure 4. Vertical velocity profile on horizontal centreline.

$P = 50$ on the top surface. Due to symmetry about the x–z plane, only half of the model is used in computation. The discretized half pipe consists of 672 linear boundary elements with 719 boundary nodes and 2880 linear cells with 2784 internal nodes. The boundary conditions are $t_x = t_y = 0$, $t_z = -50$ on the upper end, $t_x = t_y = t_z = 0$ on the lower end and $u_x = u_y = u_z = 0$ on the side surface.

Figure 7 is the plot of computed velocity vector for different cross-sections over the vertical central plane $y = 0$, where the velocity vector is scaled by multiplying by a factor of 0.3. Figure 8 is the contour plot of pressure over the vertical central plane. Table I lists the results at positions of

DOI: 10.1002/fld

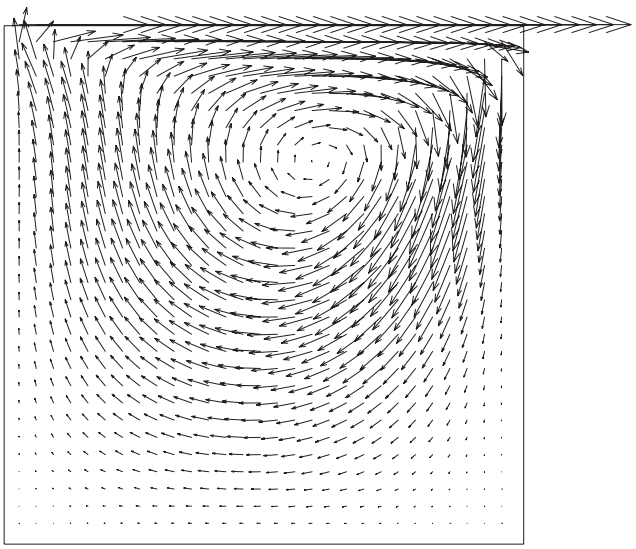

Figure 5. Velocity vector plot.

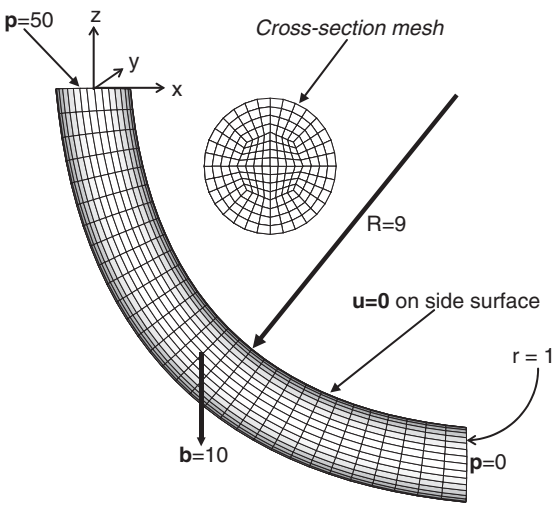

Figure 6. BEM model of the curved pipe.

maximum velocity over the different sections numbered in Figure 7. For comparison, the results obtained using CVDM [2] are also given.

From Table I, it can be seen that the velocities and pressures computed using CVDM [2] and the current formulations at the 31 cross-sections are in very good agreement. This indicates again that the derived formulations in this paper are correct. Close inspection of pressure values in Table I reveals that the pressure over the top surface (section 31) is not equal to the applied normal force

DOI: 10.1002/fld

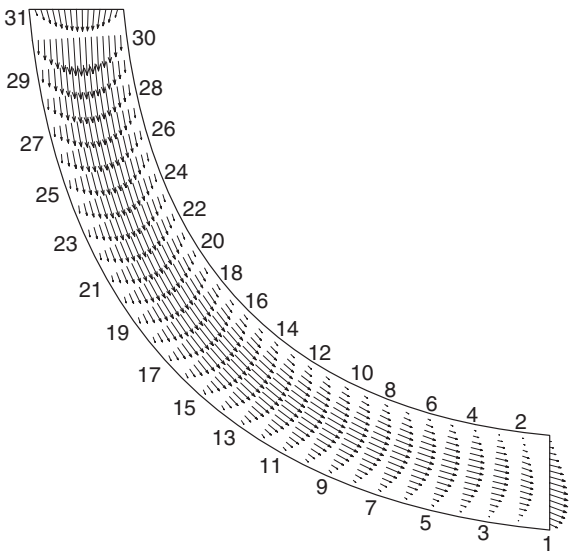

Figure 7. Scaled velocity vector plot for different sections over vertical central plane.

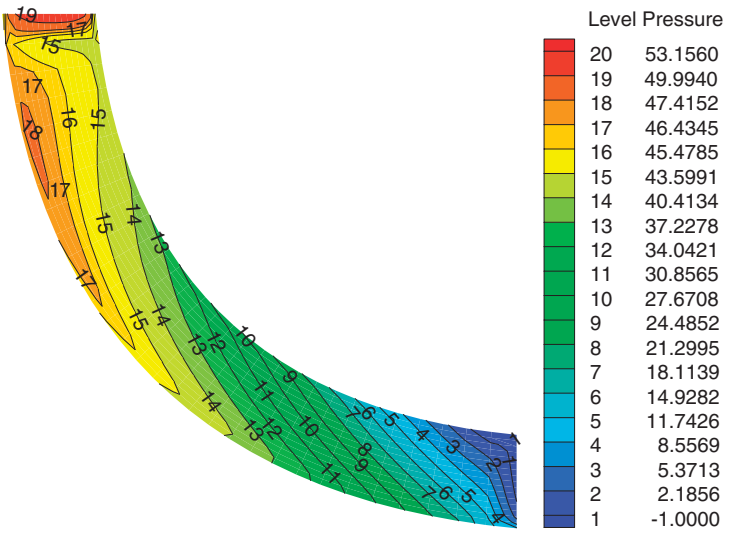

Figure 8. Contour plot of pressure over the vertical central plane.

$P = 50$. This is because the tangential velocities u_x and u_y are not zero on the top surface and therefore the computed pressure using $p = -\sigma_{ii}/3$ is not equal to the normal traction $t_z = -50$ (see Equation (4)). However, if the tangential velocities are constrained on the top surface, computed pressure will be equal to the normal traction. Interested people can find detailed information about this phenomenon in Reference [2].

DOI: 10.1002/fld

Table I. Velocities and pressures at maximum velocity position of each section over the vertical central plane $y = 0$ (see Figure 7).

Section	X	z	$\|\mathbf{u}\|$ (Current)	$\|\mathbf{u}\|$ (CVDM)	p (Current)	p (CVDM)
1	10.000	−10.250	2.0613	2.0644	−1.6257	−1.6262
3	8.8179	−9.8488	1.6212	1.6208	9.1001	9.1021
5	7.7094	−9.6240	1.8629	1.8627	16.0381	16.0389
7	6.6745	−9.3255	1.9856	1.9851	22.1191	22.1204
9	5.7133	−8.9534	2.0780	2.0778	27.2857	27.2860
11	4.8257	−8.5076	2.1621	2.1619	31.5643	31.5646
13	4.0118	−7.9882	2.2451	2.2453	35.0274	35.0271
15	3.2715	−7.3952	2.3325	2.3326	37.7732	37.7730
17	2.6048	−6.7285	2.4261	2.4259	39.9217	39.9218
19	2.0118	−5.9882	2.5266	2.5265	41.6025	41.6027
21	1.4924	−5.1743	2.6372	2.6370	42.9403	42.9407
23	1.0466	−4.2867	2.7608	2.7611	44.0435	44.0433
25	0.6745	−3.3255	2.9132	2.9137	44.9650	44.9647
27	0.3760	−2.2906	3.1421	3.1424	45.6337	45.6331
29	0.1512	−1.1821	3.6269	3.6265	45.5441	45.5448
31	0.1250	0.0000	2.3578	2.3581	53.1572	53.1565

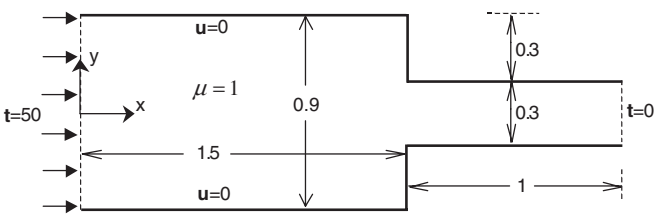

Figure 9. Geometry and boundary conditions of a sudden contraction pipe flow.

7.3. Sudden contraction pipe flow

The third example is a 2D pipe flow with a sudden contraction part (Figure 9). The fluid with the property of $\mu = 1$ and $\rho = 1$ is subjected to a pressure of $p = 50$ on the left end and is pressure free on the right end. The pipe is approximated using 202 linear boundary elements with 202 boundary nodes and 1780 internal cells with 1680 internal nodes (Figure 10). The boundary conditions applied are $t_x = 50$, $t_y = 0$ on the left end, $t_x = t_y = 0$ on the right end and $u_x = u_y = 0$ on the walls.

Figure 11 shows the computed horizontal velocity u_x along the centreline ($y = 0$) of the pipe. Figures 12–14 are the distribution of u_x over three cross-sections specified by $x = 0$, 1.5 and 2.5, respectively. For the purpose of verification, this problem is also computed using the FEM commercial software ANSYS, where a very fine mesh with 12 000 quadrilateral elements and 12 291 nodes is used and pressure boundary conditions are applied on the two ends. The ANSYS results are also shown in Figures 11–14. Figures 15 and 16 are the streamline plots for the ANSYS and the current BEM results.

From Figures 11–14, it can be seen that the BEM results are close to the results by ANSYS with a modest accuracy. The discrepancy between the results of two methods is gradually increased

DOI: 10.1002/fld

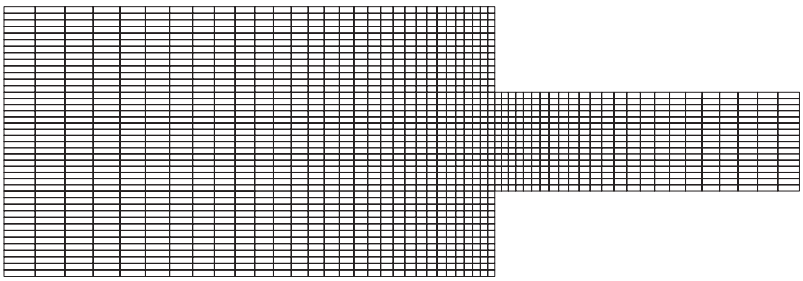

Figure 10. BEM mesh for the sudden contraction pipe flow.

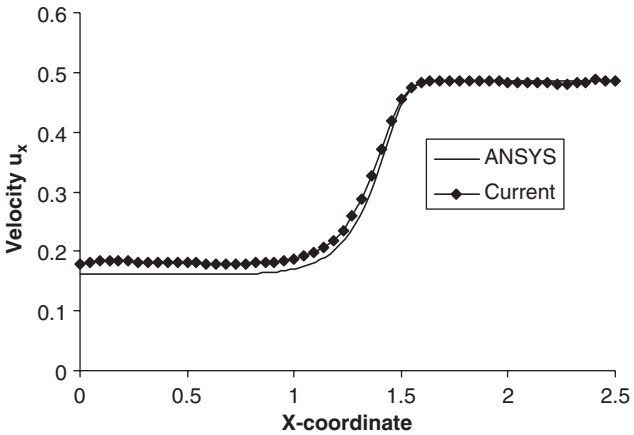

Figure 11. Horizontal velocity along the centreline of the pipe.

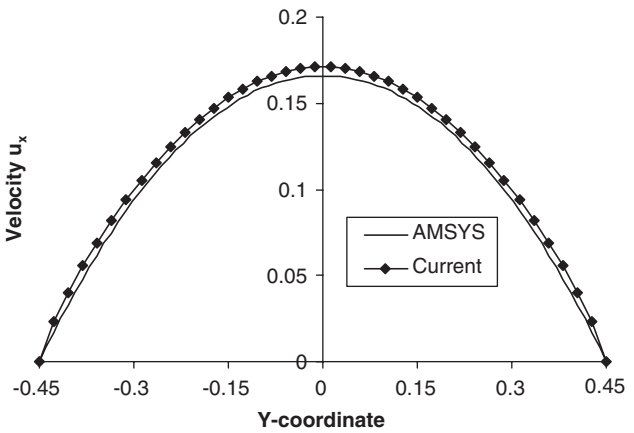

Figure 12. Horizontal velocity distribution on the left end.

DOI: 10.1002/fld

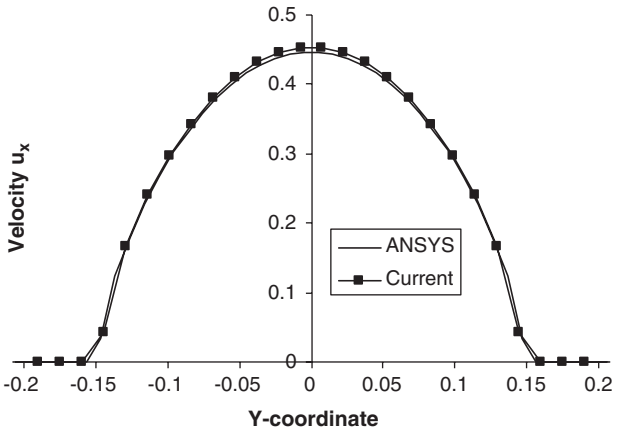

Figure 13. Horizontal velocity distribution over the shoulder section.

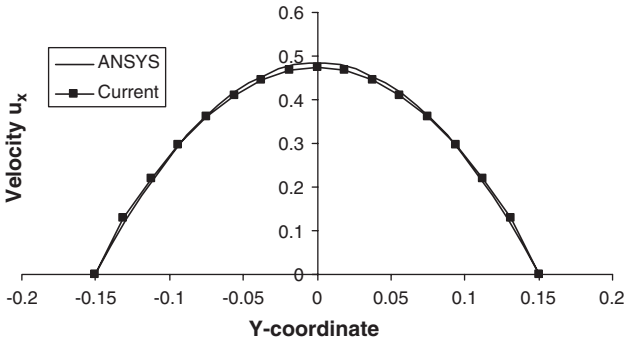

Figure 14. Horizontal velocity distribution on the right end.

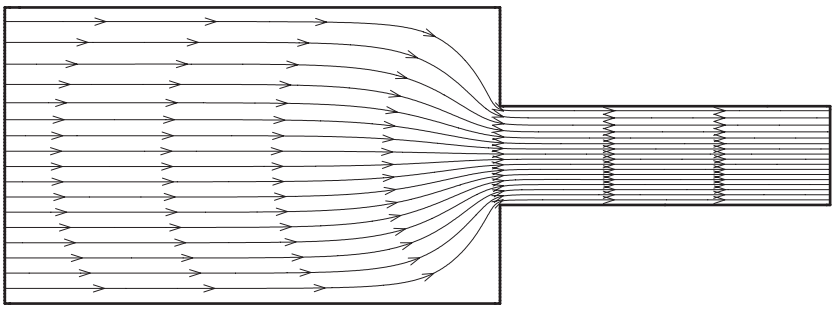

Figure 15. Streamline drawn using ANSYS results.

from right end to left end. This phenomenon is mainly due to the application of the pressure boundary conditions on the left end. In the current BEM analysis, the traction boundary condition is used, while in ANASYS computation the pressure condition is applied. As discussed in the

DOI: 10.1002/fld

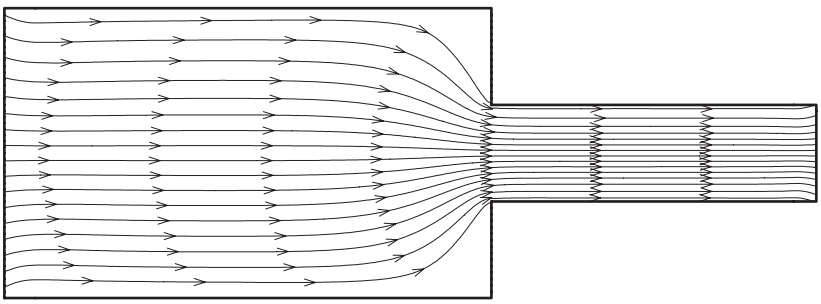

Figure 16. Streamline drawn using the current BEM results.

Table II. Computational time in different stages (minutes).

Example	Method of computation	Number of iterations	Time for evaluation of integrals	Time for forming system	Time for solving system	Total times (minutes)
Cavity	CVDM	29	3	4	10	17
	Current	28	2	4	10	16
3D pipe	CVDM	17	86	43	92	221
	Current	17	40	43	91	174
Contraction pipe	ANSYS	2500	—	—	—	14
	Current	12	2	5	12	19

previous example, the normal traction is usually not equal to the pressure of the boundary. In fact, the boundary effect can be clearly identified at the left end of the streamline plots (Figures 15 and 16). The ANSYS plot has no vertical velocity, but the BEM plot does since no velocity constraint is applied to the left end of the BEM model.

7.4. Computational time

All the examples presented above were computed on a PC computer (2 GHz, 256 Mb RAM). The computational time has been recorded for three periods [2]. The first period is from the beginning to end of the evaluation of all boundary and domain integrals. The second period refers to the forming of all matrices of system equations. And the last period is the time spent in solving the system of equations. Table II lists the computational time for the three examples described above.

Comparison of the computational times spent by CVDM and the current method in Table II shows that considerable computational time for evaluating integrals can be saved by using the current method than using CVDM, especially for 3D problems. The times listed in the fourth column of Table II consist of evaluating both the velocity integrals and velocity gradient integrals since they are computed simultaneously in the current code. If only velocity gradient integrals are computed, half and two-thirds of computational times for 2D and 3D problems, respectively, are expected to be saved by using the current method than by using CVDM. On the other hand, comparison between the current method and ANSYS in Table II shows that the BEM computation

DOI: 10.1002/fld

seems more time consuming than the FEM. This might be due to that the current BEM program was not focused on the improvement of saving computational time.

8. CONCLUDING REMARKS

A new boundary-domain integral equation for computing velocity gradients has been derived for 2D and 3D viscous flows. Full fundamental solutions for both velocity and velocity gradient integral equations are given, which show that the fundamental solutions in elasticity BEM can be reduced to ones in viscous fluid mechanics by setting the shear modulus G to the viscosity μ and Poisson's ratio v to -1.

The derived formulation is general, applicable to steady, unsteady, compressible, and incompressible flows. Three numerical examples for steady incompressible flows have demonstrated the correctness of the derived formulations.

REFERENCES

1. Gao XW. A boundary-domain integral equation method in viscous fluid flow. *International Journal for Numerical Methods in Fluids* 2004; **45**:463–484.
2. Gao XW. A promising boundary element formulation for three-dimensional viscous flow. *International Journal for Numerical Methods in Fluids* 2005; **47**:19–43.
3. Wu JC. Problems of general viscous fluid flow. *Developments in BEM* (Chapter 2), vol. 2. Elsevier: London, 1982.
4. Onishi K, Kuroki T, Tanaka M. An application of boundary element method to incompressible laminar viscous flow. *Engineering Analysis* 1984; **1**:122–127.
5. Skerget L, Alujevic A, Brebbia CA, Kuhn G. Natural and forced convection simulation using the velocity–vorticity approach. *Topics in Boundary Element Research*, vol. 5. Springer: Berlin, 1989.
6. Ramsak M, Skerget L. Mixed boundary elements for laminar flows. *International Journal for Numerical Methods in Fluids* 1999; **31**:861–877.
7. Grigoriev MM, Fafurin AV. A boundary element method for steady viscous flow using penalty formulation. *International Journal for Numerical Methods in Fluids* 1997; **25**:907–929.
8. Florez WF, Power H. Comparison between continuous and discontinuous boundary elements in the multidomain dual reciprocity method for the solution of the two-dimensional Navier–Stokes equations. *Engineering Analysis with Boundary Elements* 2001; **25**:57–69.
9. Banerjee PK, Honkala KA. Development of BEM for thermoviscous flow. *Computer Methods in Applied Mechanics and Engineering* 1998; **151**:43–62.
10. Sarler B, Kuhn G. Primitive variable dual reciprocity boundary element method solution of incompressible Navier–Stokes equations. *Engineering Analysis with Boundary Elements* 1999; **23**:443–455.
11. Power H, Mingo R. The DRM subdomain decomposition approach to solve the two-dimensional Navier–Stokes system of equations. *Engineering Analysis with Boundary Elements* 2000; **24**:107–119.
12. Zhu T, Zhang JD, Atluri SN. A local boundary integral equation (LBIE) method in computational mechanics, and a meshless discretization approach. *Computational Mechanics* 1998; **21**:223–235.
13. Sladek V, Sladek J. A new formulation for solution of boundary value problems using domain-type approximations and local integral equations. *Electronic Journal of Boundary Elements* 2003; **1**:132–153.
14. Mikhailov SE, Nakhova IS. Mesh-based numerical implementation of the localized boundary-domain integral-equation method to a variable-coefficient Neumann problem. *Journal of Engineering Mechanics* 2005; **51**:251–259.
15. Gao XW. A new inverse analysis approach for multi-region heat conduction BEM using complex-variable-differentiation method. *Engineering Analysis with Boundary Elements* 2005; **29**:788–795.
16. Gao XW, Liu DD, Chen PC. Internal stresses in inelastic BEM using complex-variable differentiation. *Computational Mechanics* 2002; **28**:40–46.
17. Gao XW. Evaluation of regular and singular domain integrals with boundary—only discetization—theory and Fortran code. *Journal of Computational and Applied Mathematics* 2005; **175**(2):265–290.

DOI: 10.1002/fld

18. White FM. *Viscous Fluid Flow* (2nd edn). McGraw-Hill: Boston, 1991.
19. Brebbia CA, Dominguez J. *Boundary Elements*: *An Introductory Course*. McGraw-Hill: London, 1992.
20. Gao XW, Davies TG. *Boundary Element Programming in Mechanics*. Cambridge University Press: Cambridge, 2002.
21. More JB, Hillstrom K. *User Guide for MINPACK-1*. *Argonne National Labs Report ANL80-74*, Argonne, IIIinois, 1980 (Program HYBRJ can be downloaded from: http://netlib.org/minpack/).
22. Ghia U, Ghia KN, Shin CT. High-Re solutions for incompressible flow using the Navier–Stokes equations and a multigrid method. *Journal of Computational Physics* 1982; **48**:387–411.

DOI: 10.1002/fld